



Cite this: *Biomater. Sci.*, 2020, **8**, 1127

## Biomimetic proteoglycan nanoparticles for growth factor immobilization and delivery†

Nooshin Zandi,<sup>a,b</sup> Ebrahim Mostafavi,<sup>b</sup> Mohammad Ali Shokrgozar,<sup>c</sup> Elnaz Tamjid,<sup>d</sup> Thomas J. Webster,<sup>b</sup> Nasim Annabi<sup>b</sup> \*e,f,g and Abdolreza Simchi<sup>a,h</sup>

The delivery of growth factors is often challenging due to their short half-life, low stability, and rapid deactivation. In native tissues, the sulfated residual of glycosaminoglycan (GAG) polymer chains of proteoglycans immobilizes growth factors through the proteoglycans'/proteins' complexation with nanoscale organization. These biological assemblies can influence growth factor–cell surface receptor interactions, cell differentiation, cell–cell signaling, and mechanical properties of the tissues. Here, we introduce a facile procedure to prepare novel biomimetic proteoglycan nanocarriers, based on naturally derived polymers, for the immobilization and controlled release of growth factors. We developed polyelectrolyte complex nanoparticles (PCNs) as growth factor nanocarriers, which mimic the dimensions, chemical composition, and growth factor immobilization of proteoglycans in native tissues. PCNs were prepared by a polymer–polymer pair reaction method and characterized for physicochemical properties. Fourier transform infrared spectroscopy (FTIR) analysis indicated that complexation occurred through electrostatic interactions. Transmission electron microscopy (TEM) results showed that the nanocarriers had a diameter of  $60 \pm 11$  nm and  $91 \pm 33$  nm for dermatan sulfate sodium salt–poly-L-lysine (DS-PLL) and gum tragacanth–poly-L-lysine (GT-PLL) complexes, respectively. The colloidal nanoparticles were stable due to their negative zeta potential, *i.e.*  $-25 \pm 4$  mV for DS-PLL and  $-18 \pm 3.5$  mV for GT-PLL. Cytocompatibility of PCNs in contact with human bone marrow stromal cells (HS-5) was confirmed through a live/dead assay and metabolic activity measurement. In addition, vascular endothelial growth factor (VEGF) was used to evaluate the ability of PCNs to stabilize growth factors. The capability of PCNs to preserve VEGF activity for up to 21 days was confirmed by analyzing the metabolic and mitogenic characteristics of human umbilical vein endothelial cells (HUVECs). Our results demonstrated the potential applications of these nanoparticles in therapeutic delivery for tissue regeneration applications.

Received 27th April 2019,  
Accepted 15th July 2019

DOI: 10.1039/c9bm00668k

rsc.li/biomaterials-science

<sup>a</sup>Institute for Nanoscience and Nanotechnology, Sharif University of Technology, P.O. Box 11365-11155, Tehran, Iran. E-mail: simchi@sharif.edu; Tel: +98 (21) 6616

<sup>b</sup>Department of Chemical Engineering, Northeastern University, Boston, 02115, USA

<sup>c</sup>National Cell Bank Department, Pasteur Institute of Iran, Tehran 13164, Iran

<sup>d</sup>Department of Nanobiotechnology, Faculty of Biological Sciences Tarbiat Modares University, P.O. Box 14115-175, Tehran, Iran

<sup>e</sup>Department of Chemical and Biomolecular Engineering, University of California – Los Angeles, Los Angeles, California 90095, USA. E-mail: nannabi@UCLA.edu; Tel: +1 (310) 267-5927

<sup>f</sup>Center for Minimally Invasive Therapeutics (C-MIT), California NanoSystems Institute (CNSI), University of California – Los Angeles, 570 Westwood Plaza, Los Angeles, CA 90095, USA

<sup>g</sup>Harvard-MIT Division of Health Sciences and Technology, Massachusetts Institute of Technology, Cambridge, MA 02139, USA

<sup>h</sup>Department of Materials Science and Engineering, Sharif University of Technology, P.O. Box 11365-11155, Tehran, Iran

† Electronic supplementary information (ESI) available. See DOI: 10.1039/c9bm00668k

## Introduction

During the past decade, considerable efforts have been made to enhance the bioavailability and biocompatibility of therapeutic agents.<sup>1</sup> Among the different delivery carriers, polyelectrolyte complexes have attracted great attention due to their well-tolerated properties and potential as delivery vehicles for drugs, enzymes and proteins, and DNA encapsulation.<sup>2</sup> Polyelectrolyte complexes are appropriate for loading charged drug molecules due to the simple fabrication process, high drug loading efficiency and efficacy, acceptable structural stability, and extended circulation in the blood.<sup>3</sup>

Polyelectrolyte complex structures are made by complexation of oppositely charged biopolymers in solution at the molecular level, generally *via* formation of hydrogen bonds, and electrostatic and hydrophobic interactions.<sup>4–7</sup> Electrostatic interactions are important intermolecular forces for complex oppositely charged polymers, which are derived by entropic

changes through the release of bound counterions.<sup>8</sup> Under non-stoichiometric compositions, nanoparticles (NPs) with a net charge of the excess component, are formed.<sup>9</sup> Polyelectrolyte complex nanoparticles (PCNs) derived from naturally derived polymers are promising vehicles for active targeting delivery because natural polymers intrinsically have cell binding sites and exhibit high biocompatibility.<sup>10,11</sup> For example, negatively charged polysaccharides, such as carboxymethyl cellulose,<sup>12</sup> dextran sulfate,<sup>13</sup> alginate,<sup>3</sup> and chondroitin sulfate,<sup>14</sup> have been complexed with positively charged polymers to generate PCNs for drug delivery.<sup>15</sup>

Glycosaminoglycans (GAG) include different types of long linear polysaccharide chains containing chondroitin sulfate (CS), keratan sulfate (KS), dermatan sulfate (DS), heparin (HP), hyaluronic acid (HA), and heparin sulfate (HS).<sup>16</sup> In addition, GAGs have various negatively charged carboxyl and sulfate groups that can maintain water in tissues and can be used as therapeutic agents for the treatment of osteoarthritis, cancer, bacterial and viral infections, and blood clotting. These biopolymers can regulate cell signalling, migration, and differentiation through specific interactions with various ligands. Sulfated GAG is often covalently bound to a protein to form proteoglycans (PG), which derives its function from the GAG side chain.<sup>17</sup>

In native tissues, growth factor stabilization and delivery to cells are driven by various stimuli through complex microenvironments. Therefore, the biomimetic milieu enables growth factor stabilization and delivery, simultaneously. The GAG side chains of different proteoglycans are responsible for growth factor stabilization and protection, and signal regulation through linkage with cell surface receptors.<sup>18–20</sup> This motivates the usage of GAG as a carrier for growth factors. Proteoglycans have a wide range of sizes, with a core protein ranging from 20 to 400 kDa, and GAG side chains from one or two side chains such as decorin and biglycan to over 100 side chains like aggrecan. These structures display nanoscale organizations.<sup>21</sup> Therefore, in addition to the chemical functions of proteoglycans, their nanoscale structures play a crucial role in their biophysical function.<sup>21–24</sup>

Gum tragacanth (GT) is another biocompatible and biodegradable polysaccharide which has been used for the preparation of delivery vehicles.<sup>25</sup> At the near neutral pH, carboxyl groups of GT are dissociated, forming negative charges to interact with positively charged polymers such as poly-L-lysine (PLL).<sup>26</sup> PLL and its derivatives, such as homo-poly-amino acid, are an important class of biodegradable cationic polymers for biomedical and pharmaceutical applications. They have extensively been studied and utilized as auxiliary agents in drug delivery systems.<sup>27</sup>

Different PCNs have been formed by complexing biopolymers, including combinations of chitosan with different negatively charged polymers such as dextran sulfate,<sup>28</sup> hyaluronic,<sup>29</sup> alginate<sup>30</sup> or heparin.<sup>31</sup> PCNs could be used to preserve growth factors from degradation by enzymes along with the desired release profile. In addition, their nanoscale size allows crossing of the epithelium.<sup>32</sup> Huang *et al.* investigated the mito-

genic properties of vascular endothelial growth factor (VEGF) using VEGF-PCN complexation up to five days. They used dextran sulfate as the anionic polymer with different polycations, including PLL, chitosan, and poly-(ethyleneimine), to prepare the PCNs.<sup>33</sup> Incorporation of chitosan-heparin NPs with a decellularized vein scaffold was reported in order to promote vascularization in the scaffold through localizing VEGF. Results revealed that controlled release of VEGF over 30 days could increase cellular proliferation and infiltration, extracellular matrix (ECM) generation, and vascularization.<sup>31</sup>

In addition to the excess attention to other polysaccharides such as heparin,<sup>34</sup> dermatan sulfate (DS) functions as a cofactor in a variety of therapeutics, especially in cell-mediated tissue regeneration. This biopolymer plays an important role in binding to and activating extracellular molecules and growth factors for numerous essential biological processes, including cell adhesion, migration, proliferation and differentiation.<sup>30</sup> However, so far, the use of DS in clinical trials as a drug delivery platform for promoting therapeutic functions is limited. Herein, we use VEGF as a model growth factor due to its short circulation half-life. Also, binding to PCNs could influence its stability and presentation to growth factor receptors.<sup>33,35</sup> In addition, it has been reported that modified VEGF with these ECM-binding motifs improved healing in chronic diabetic wounds and bone defects.<sup>36</sup>

In the current study, we developed polyelectrolyte NPs that mimic the size and biochemical function and chemistry of proteoglycans for VEGF protection and immobilization. Biomimetic proteoglycan NPs were prepared through a combination of PLL as the polycationic element and two anionic polysaccharides of GT and dermatan sulfate sodium salt (DS). The engineered NPs were characterized by size distribution, zeta potential, surface functional groups, and cytocompatibility against human bone marrow stromal cells (HS-5). The ability of the PCNs to preserve VEGF activity was investigated by measuring the metabolic and mitogenic characteristics of human umbilical vein endothelial cells (HUVECs) in the presence of PCNs.

## Results and discussion

The nanocarrier was formed by the interaction between the dissociated functional groups: an anionic sulfonate group ( $-\text{OSO}_3^-$  in the dermatan sulfate polymer) and carboxyl group ( $-\text{COO}^-$  in GT) with a cationic amino group ( $-\text{NH}_3^+$ ) from PLL without cross-linking, or the use of a surfactant organic solvent. The physical characteristics (hydrodynamic particle size, zeta potential, and polydispersity index (PDI)) of PCNs with different polycation: polyanion mixing ratios in DI water are shown in Table 1. Fig. 1 demonstrates the schematic for the chemical building units of the polymers and their interactions to form complex NPs. The process yield was  $41 \pm 6\%$  for DS-PLL and  $30 \pm 5\%$  for GT-PLL. Zeta potential indicated the negatively charged PCNs (Table 1). The colloidal NPs in DI water were deemed stable due to their negative zeta potential, *i.e.* of  $-25 \pm 4$  mV (DS-PLL) and  $-18 \pm 3.5$  mV (GT-PLL). These

**Table 1** Hydrodynamic diameter ( $D_h$ , nm), polydispersity index (PDI), and zeta potential ( $\zeta$ , mV) for DS-PLL and GT-PLL PCNs prepared at different charge mixing ratios

$V_{PA} : V_{PC}$	Property	DS-PLL	GT-PLL
1 : 5	$D_h$	$222 \pm 8$	$402 \pm 4$
	PDI	$0.11 \pm 0.02$	$0.13 \pm 0.05$
	$\zeta$	$-27 \pm 4$	$-20 \pm 3$
1 : 6	$D_h$	$105 \pm 0.5$	$376 \pm 3$
	PDI	$0.12 \pm 0.05$	$0.13 \pm 0.02$
	$\zeta$	$-25 \pm 4$	$-19 \pm 2.5$
1 : 7	$D_h$	$107 \pm 3.5$	$304 \pm 6$
	PDI	$0.2 \pm 0.08$	$0.32 \pm 0.07$
	$\zeta$	$-21 \pm 3$	$-18.5 \pm 3$
1 : 10	$D_h$	$102 \pm 9$	$220 \pm 2$
	PDI	$0.338 \pm 0.3$	$0.22 \pm 0.08$
	$\zeta$	$-19 \pm 2$	$-18 \pm 3.5$

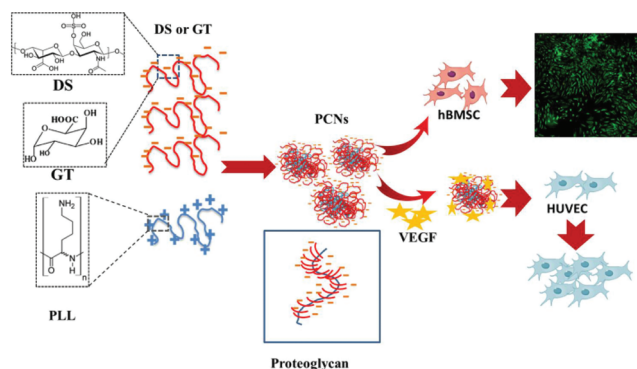


**Fig. 1** Schematic representation of nanoparticle formation and their interaction with the cells. Polyelectrolyte nanoparticles were formed by the complexation of polycationic PLL (blue) with the polyanionic DS or GT (red) in excess. These NPs have similar size and composition of the proteoglycans in the body. PCNs were exposed to hBMSCs to evaluate their cytocompatibility. The mitogenic and metabolic activity of immobilized VEGF on the PCNs was also evaluated by using HUVECs.

structures might form a core/shell configuration, where the excess polymer in the polyelectrolyte component is located in the shell, giving the particle the defined charge sign and colloid stability. The negatively charged PCNs could easily bind to the positively charged drug and growth factors, which makes them suitable candidates for delivery of therapeutics. This method is suitable for encapsulating materials sensitive to different stress factors such as proteins. The characteristics of the prepared nanocarriers and their potential to immobilize VEGF and preserve the growth factor activity were then studied.

### The size and morphology of the PCNs

Representative scanning electron microscopy (SEM) and transmission electron microscopy (TEM) images of PCNs and their size distribution histogram are shown in Fig. 2a–f. These analyses indicated individual spherical particles with an average

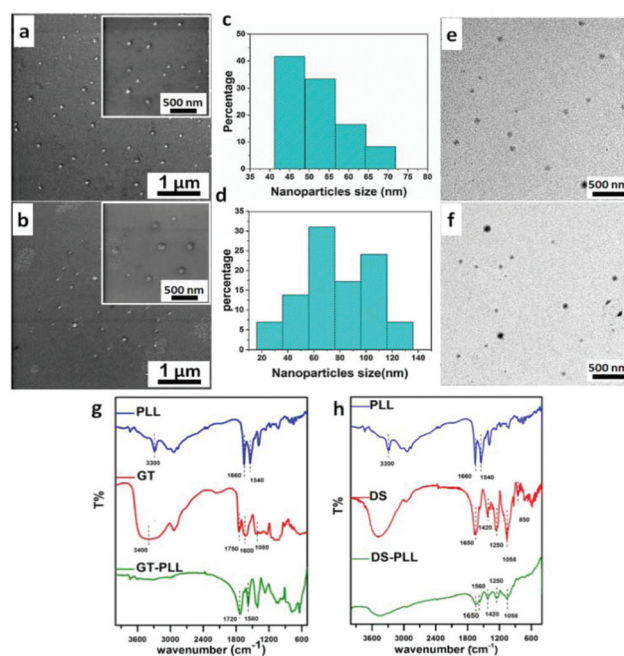


**Fig. 2** Characterization of PCNs. Representative scanning electron microscopy (SEM) images of negatively charged (a) DS-PLL and (b) GT-PLL NPs. Size histograms for (c) DS-PLL and (d) GT-PLL by measuring the mean diameters of the NPs using ImageJ software (National Institute of Health, Bethesda, MD). Representative transmission electron microscopy (TEM) images of (e) DS-PLL and (f) GT-PLL NPs. FTIR spectra of (g) raw materials (DS, PLL, and GT) and (h) the synthesized NPs.

diameter of  $60 \pm 11$  nm and  $91 \pm 33$  nm for DS-PLL and GT-PLL NPs, respectively. Also, SEM and TEM images of VEGF-loaded PCNs are shown in Fig. 1Sa–d.† These analyses indicated individual spherical particles with an average diameter of  $55 \pm 8$  nm and  $103 \pm 29$  nm for DS-PLL-VEGF and GT-PLL-VEGF NPs, respectively.

Based on the DLS data reported in Table 1, we selected 1 : 6 and 1 : 10 as the optimum polycation : polyanion mixing ratios for DS-PLL and GT-PLL, respectively, due to the optimum values for PDI, hydrodynamic size and zeta potential of NPs. The result showed a hydrodynamic size of  $105 \pm 0.5$  nm for DS-PLL and  $220 \pm 2$  nm for GT-PLL with monomodal size distribution. The larger size of the GT-PLL NPs can be attributed to the higher molecular weight of GT (180 kDa) as compared to DS (84 kDa). It is important to mention that the complex NPs in the solution do not behave like hard spheres, but rather they are gel-like or have a solid core surrounded by a charged corona.<sup>37</sup> TEM can be used to observe the NPs in the dry state; however, dynamic light scattering (DLS) enables to detect the NPs in a solvent. Therefore, the DLS method indicates the hydrodynamic diameter of particles, including the core with any molecules attached to or adsorbed on the surface. Solvent molecules bind to the particles through different non-covalent interactions such as van der Waals interactions, hydrogen bonding or  $\pi$ - $\pi$  stacking. The size of the particles measured by DLS depends on the type of the

solvent. Different solvents ensure different solvation characteristics. Water, which is the PCNs' media, acts as both a hydrogen bond donor and acceptor. The hydrogen bond is a specific type of strong non-covalent interaction that includes dipole-dipole attraction between a partially positive hydrogen atom and a partially negative oxygen, nitrogen, sulfur, or fluorine atom. Therefore, as expected, the particle sizes measured by the DLS method were slightly bigger than those measured *via* TEM and SEM images.

On the other hand, the zeta potential of DS-PLL was slightly lower ( $-25 \pm 4$  mV) than that of GT-PLL ( $-18 \pm 3.5$  mV). This observation indicates that anionic PCNs were formed. Nevertheless, DS has strong anionic sulfate groups, while GT is a mild anionic polysaccharide. Therefore, DS-PLL NPs showed a lower zeta potential. The size, PDI, and zeta potential of PCNs after growth factor loading are reported in Table 2. The magnitude of the zeta potential substantially dropped after incorporation of VEGF in the PCNs for both types of the PCNs, whereas the hydrodynamic size of the PCNs did not show significant changes after loading of VEGF.

In addition, DLS analysis of DS-PLL and GT-PLL with 1 : 6 and 1 : 10 mixing ratios of polycation : polyanion in cell culture media is reported in Table 2. The average size distribution of the particles suspended in the cell culture media was greater than that in DI water. This indicates that PCNs formed larger complexes in the media. To that end, the PDI of the particles suspended in the media were higher than that of those suspended in DI water, implying that the PCNs in the culture media had broader size distributions. Suspension of the PCNs in the culture media yielded a lower surface charge density. The electrostatic binding can explain the interaction between the proteins in the culture media and negatively charged PCNs. On the other hand, the lower surface charge density of the PCNs in the culture media might be derived from adsorption of uncharged or positively charged amino acids (*e.g.* L-glutamine in blood serum).

Furthermore, to evaluate the stability of PCNs under optimized conditions (a concentration of  $1 \text{ mg ml}^{-1}$  in acetate buffer with 0.1 M and pH = 5.5), the hydrodynamic diameter and zeta potential of NPs were measured 1, 3 and 14 days after incubation at room temperature. As shown in Fig. 3, no significant changes in the hydrodynamic size of the PCNs were observed. In addition, the zeta potential value remained the same after 14 days.

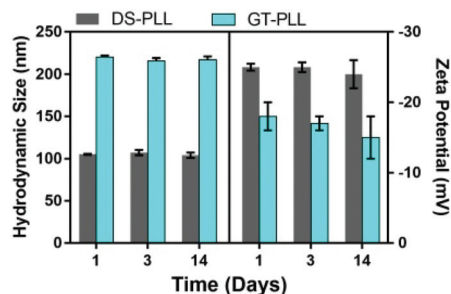


Fig. 3 Hydrodynamic diameter (nm) and zeta potential (mV) for DS-PLL and GT-PLL PCNs after 1, 3, and 14 days of incubation in acetate buffer (pH = 5.5) at room temperature (25 °C).

### Fourier transform infrared spectroscopy

FTIR spectra of pristine GT, PLL, and DS polymers and the NPs (GT-PLL and DS-PLL) are shown in Fig. 2g and h. Two features were prominent in the spectrum of PLL, absorbance in the range  $3300 \text{ cm}^{-1}$  and the bands near  $1500\text{--}1600 \text{ cm}^{-1}$ . The band at  $1620\text{--}1700 \text{ cm}^{-1}$  was attributed to amide I (mainly the CO stretching mode) and the band at  $1540 \text{ cm}^{-1}$  (amide II) was related to the in-plane deformational mode of the NH group.<sup>38</sup> Both bands were related to the vibrational modes of the peptide group. Bands at  $1650$  and  $1429 \text{ cm}^{-1}$  in the FTIR spectrum of DS were related to axial symmetrical and asymmetrical deformations of carboxylate anions, respectively.<sup>39</sup> The bands at  $1250$  and  $850 \text{ cm}^{-1}$  were attributed to the axial asymmetry of S=O groups and the axial deformation of C-O-S.<sup>40</sup> Major absorbance bands in GT appeared at  $3415 \text{ cm}^{-1}$  (stretching vibrations of O-H groups),  $2945 \text{ cm}^{-1}$  (stretching vibrations of methylene groups),  $1750 \text{ cm}^{-1}$  (various carbonyl species),  $1620 \text{ cm}^{-1}$  (carbonyl stretching vibrations in carboxylic acids),  $1417 \text{ cm}^{-1}$  (symmetrical stretch of carboxylate group),  $1244$  and  $115 \text{ cm}^{-1}$  (C-O stretching vibrations of polyols), and  $1080$  and  $1024 \text{ cm}^{-1}$  (C-O stretching vibrations of ether and alcohol groups).<sup>37</sup> After complexation, peak shifts, the appearance of new peaks and/or disappearance of some characteristic peaks, were observed.

In DS-PLL, shifting of the band at  $1660 \text{ cm}^{-1}$  to  $1560 \text{ cm}^{-1}$  was observed due to vibrations of the residual N-H<sup>+</sup> bonds in PLL. Based on a previous study,<sup>41</sup> electrostatic interactions between PLL and DS can be verified over spectra analysis at  $1520$  to  $1560 \text{ cm}^{-1}$ . These bands in the FTIR spectra of the PCNs showed reduced intensity. The complexation of COO<sup>-</sup> in the DS chains with cationic moieties in the PLL polymer chains can be an explanation of this effect. Electrostatic interactions between NH<sub>3</sub><sup>+</sup> of PLL with -OSO<sub>3</sub><sup>-</sup> groups of DS contributed to the formation of an anionic-cationic polymer complex. Additional evidence could be the disappearance of the band at  $850 \text{ cm}^{-1}$  for DS after complexation. Instead, the intensity of a  $1250 \text{ cm}^{-1}$  band was enhanced as compared to DS. Similar changes were noticed in the FTIR spectrum of GT-PLL. The complexed material showed a narrower band around  $3300 \text{ cm}^{-1}$ , due to new hydrogen bonds forming between -OH and -NH<sub>2</sub> functional groups of PLL and -C=O

Table 2 PCN characterization in DI water and cell culture media

Particle media	Composition	Particle size (nm)	PDI	Zeta potential (mV)
DI water	DS-PLL	105 ± 0.5	0.12 ± 0.05	-25 ± 4
	DS-PLL-VEGF	98 ± 7	0.28 ± 0.05	-11.20 ± 3
	GT-PLL	220 ± 2	0.22 ± 0.08	-18 ± 3.5
	GT-PLL-VEGF	212 ± 9	0.36 ± 0.03	-5 ± 2
Cell culture media	DS-PLL	118.6 ± 4.1	0.411 ± 0.04	-11.43 ± 3
	GT-PLL	290 ± 3.5	0.324 ± 0.06	-5.17 ± 3.8

and -OH functional groups of GT.<sup>42</sup> On the other hand, the bands assigned to motions of -NH<sub>2</sub> at 3300 cm<sup>-1</sup> became invisible after complexation. This disappearance could be related to the lower content of PLL and GT excess in the complex NPs. Intense peaks at around 1580 cm<sup>-1</sup> and 1720 cm<sup>-1</sup> were also present. The peak at 1720 cm<sup>-1</sup> probably corresponded to asymmetric stretching of -COO<sup>-</sup> groups that might indicate polyelectrolyte complex development. Based on FTIR analysis, it can be concluded that ionic bonds between PLL amine groups and the carboxyl group of GT were formed, which is in agreement with a previous study.<sup>43</sup>

### Cytocompatibility assays

To determine the *in vitro* cytocompatibility of the PCNs, a live/dead assay and metabolic activity measurement were performed after exposing human bone marrow stromal cells (HS-5) to the engineered PCNs. Three doses of the PCNs (200, 400, and 800 µg mL<sup>-1</sup>) were compared to the untreated cells as a negative control (cells in the culture medium without the NPs). Representative live/dead stained images of the cells treated with the PCNs as compared to the controls are shown in Fig. 4a. The live/dead assay stains the dead cells in red and the live cells in green. For both type of the PCNs, the viability significantly decreased (to less than 50%), as the concentration

of the NPs increased to higher 400 µg mL<sup>-1</sup>. This drop in cell viability at a higher concentration indicated their cytotoxicity at high concentrations (Fig. 4b).

A PrestoBlue® assay was carried out to evaluate the cellular metabolic activity at three dose levels of 200, 400 and 800 µg mL<sup>-1</sup>, at days 1, 3 and 5 post culture. As shown in Fig. 4c, no statistical difference between the NPs at 200 µg mL<sup>-1</sup> and control was observed. Additionally, the results revealed that at higher concentrations of the NPs (e.g. 400 and 800 µg mL<sup>-1</sup>), the metabolic activity of the cells decreased consistently during 5 days of culture. At NP concentrations higher than 400 µg mL<sup>-1</sup>, the NPs could prevent attachment of the cell to the surface of the well plate.

### Cell response to VEGF and preconditioned VEGF-loaded PCNs

The ability of PCNs to preserve VEGF activity was evaluated by exposing the pre-conditioned VEGF-loaded PCNs and uncomplexed VEGF for 7 and 14 days to HUVECs at 37 °C in the culture media. We used 10 ng mL<sup>-1</sup> VEGF and 100 µg mL<sup>-1</sup> PCNs as the final concentrations. The VEGF loading efficiency was 93.1 ± 5% and 80.2 ± 3% for DS-PLL and GT-PLL, respectively. Since there was no step to remove free VEGF, each experiment (mitogenic and metabolic activity experiments) used an equal amount of VEGF. Regarding the negative control (no VEGF), HUVECs did not proliferate under these low-serum

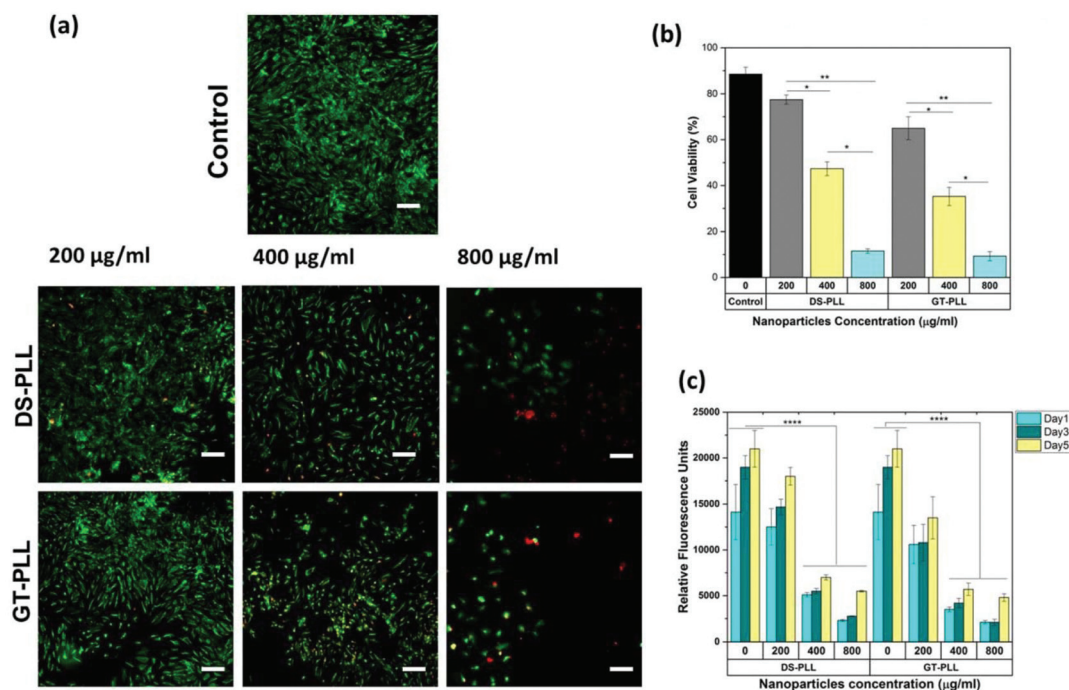


**Fig. 4** *In vitro* cytocompatibility of the polyelectrolyte NPs against HS-5 cells. (a) Representative live/dead stained images, indicating the effect of PCN (DS-PLL and GT-PLL) dose on the cell viability at day 3 post seeding. The concentration of NPs increases from 200 to 800 µg mL<sup>-1</sup> from left to right. Cytotoxicity was observed for the cells treated with NPs at concentrations >400 µg mL<sup>-1</sup>. (b) Quantification of cell viability after 24 h of incubation. (c) Quantification of metabolic activity of hBMSCs based on relative fluorescence units (RFU) at different incubation times (1, 3 and 5 days post seeding). Scale bars: 100 µm. Results are presented as the mean ± STD with at least three replicates per group. The significance levels are shown as  $p < 0.05$  (\*),  $p < 0.01$  (\*\*), and  $p < 0.0001$  (\*\*\*) for  $n = 3$ .

conditions after 48 h of cell culture. Representative DAPI-stained images in Fig. 5a show cell nuclei culturing in the low-serum media for both VEGF bound to PCNs (DS-PLL and GT-PLL) and VEGF in solution after 7 and 14 days. The number of cells was normalized and compared for both VEGF bound to PCNs and free VEGF in Fig. 5b. As the results show, the untreated cells did not proliferate in the low-serum media. Cell proliferation was observed for free VEGF but was significantly lower than that of the treated cells with PCN-bound VEGF. The normalized cell numbers for the free VEGF was statistically lower than VEGF bound to PCNs (for both DS-PLL and GT-PLL) in both pre-conditioning times. However, these values were not statistically significant compared to the negative control. In addition, the normalized cell numbers were more than 1 for both of the treatments with VEGF (bound and free VEGF), indicating that the cell numbers were enhanced as compared to the cells cultured without the growth factor. The mitogenic activity of VEGF bound to DS-PLL was also more than that of VEGF bound to GT-PLL at each time point. It can be concluded that treatment with VEGF bound to PCNs (for both DS-PLL and GT-PLL) represents mitogenic activity over the 14 days of pre-conditioning in the high level, while free

VEGF lost mitogenic activity by increasing the pre-conditioning time.

The MTT assay was used to investigate the cellular responses to pre-conditioned VEGF during mitosis experiments for 48 h. Fig. 5c demonstrates the results of the metabolic activity for both types of VEGF-containing treatments. VEGF bound to each type of PCNs demonstrated no statistical differences over all pre-conditioning times. This result indicates that based on the metabolic activity of treatments, VEGF activity did not change during pre-conditioning. However, free VEGF treatment showed a significant reduction in metabolic activity after 21 days in comparison with 7 days of pre-conditioning. At day 7 of pre-conditioning, there was no statistical difference between free and treated VEGF groups. However, by increasing the pre-conditioning time, loss of metabolic activity of HUVECs was observed. VEGF-bound DS-PLL showed a higher metabolic activity in comparison with free VEGF even after 14 days of incubation, but there was no significant difference between VEGF-bound GT-PLL and free VEGF at this time point. Finally, after 21 days of pre-conditioning time, the metabolic activity of both PCNs treatments was greater than that of VEGF alone.

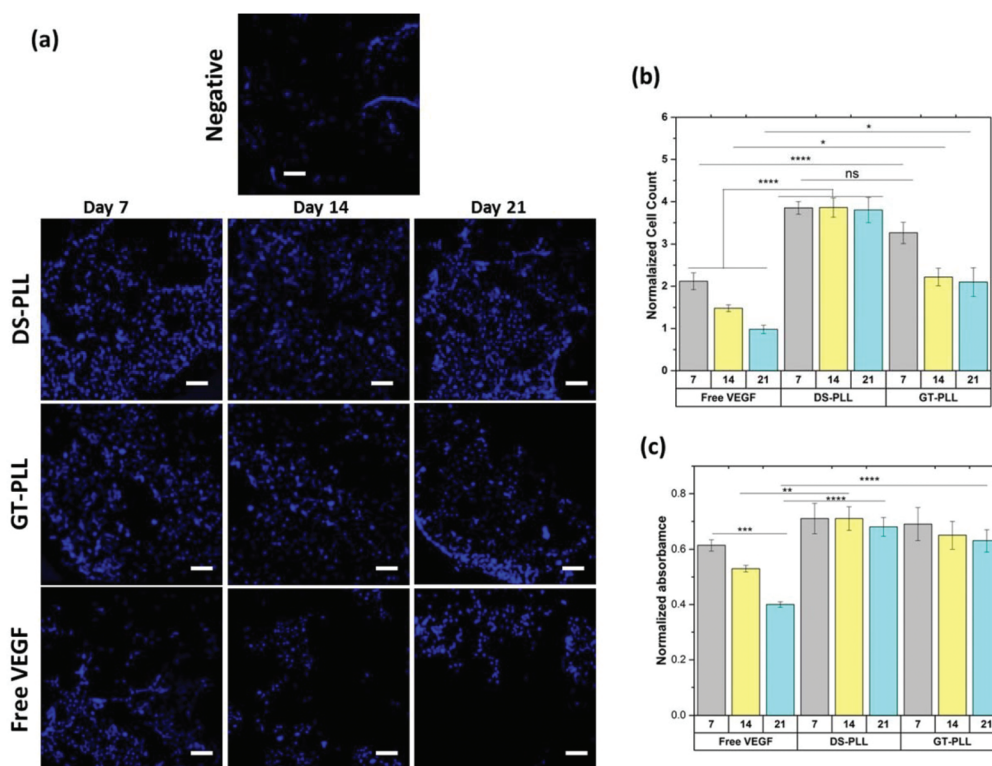


**Fig. 5** Cell response to VEGF and pre-conditioned VEGF-loaded PCNs through mitogenic and metabolic measurements. (a) Representative fluorescence images of HUVEC nuclei stained with DAPI after 2 days of culture with no treatment (negative control), VEGF-loaded PCNs (DS-PLL and GT-PLL), and free VEGF. Pre-conditioning time does not show a significant influence on mitogenic activity, but the treatments exhibit significant effects. (b) Quantification of VEGF mitogenic activity after 2 days of HUVEC culture for VEGF-loaded PCNs and free VEGF. The numbers represent cell counts normalized to cell counts from the negative control. (c) The quantification of metabolic activity after 2 days of culture with VEGF-loaded PCNs and free VEGF in solution (at different pre-conditioning times in the media up to 21 days). Metabolic activity result was normalized to the metabolic activity of untreated HUVEC cells. Scale bars: 100 μm. Results are presented as the mean ± SEM with at least three replicates per group. The significance levels are shown as  $p < 0.05$  (\*),  $p < 0.01$  (\*\*),  $p < 0.001$  (\*\*\*), and  $p < 0.0001$  (\*\*\*\*) for  $n = 3$ .

Since free VEGF in solution exhibited a significantly lower mitogenic and metabolic activity compared to VEGF bound to both types of PCNs, the PCNs could be mainly responsible for the high level activity of the growth factor. For the DS-PLL PCNs, VEGF molecules could link to the PCNs over the pre-conditioning time which, corresponds to the higher mitogenic activity of this treatment. In addition, both PCN treatments induced more metabolic activity at all pre-conditioning times compared to the negative control, indicating that VEGF remained active during the 21 days (Fig. 5c). Both GT and DS biopolymers are highly negatively charged polysaccharides that can bind to VEGF electrostatically. However, the glycosaminoglycan used in this work consisted of primarily 6-Osulfated hexosamine and iduronic residue, which are important for binding to VEGF<sup>44,45</sup> and lack the particular VEGF-binding sulfation, making GT less effective at stabilizing VEGF.

## Experimental

### Materials

DS (from porcine intestinal mucosa,  $\geq 90\%$ , lyophilized powder 60 kDa; PDI = 1.94) and PLL (0.1% (w/v) in H<sub>2</sub>O) were purchased from Sigma-Aldrich (St Louis, MO, USA). Sodium acetate, sodium chloride, potassium chloride, sodium phosphate dibasic, and potassium phosphate monobasic were purchased from Merck (Germany). GT used in this study was a high-quality ribbon type, collected from the stems of *floccosus* species of *Astragalus* bushes, grown in the central areas of Iran. A live/dead viability/cytotoxicity kit for mammalian cells was purchased from Invitrogen (Eugene, OR). The PrestoBlue reagent and Dulbecco's phosphate buffered saline (DPBS) were purchased from Thermo Fisher Scientific. VEGF was purchased from R&D Systems, and MTT (3-[4,5-dimethylthiazol-2-yl]-2,5-diphenyltetrazolium bromide), 4',6-diamidino-2-phenylindole (DAPI), bovine serum albumin (BSA), and paraformaldehyde were purchased from Sigma-Aldrich (St Louis, MO, USA).

### Preparation of PCNs

PCNs were prepared through the drop by drop mixing of a polycation solution with a polyanion solution and stirring vigorously with an excess amount of the polyanion. Two different combinations of polycation–polyanion were used to form the PCNs, including dermatan sulfate with poly-L-lysine (DS-PLL), and gum tragacanth with poly-L-lysine (GT-PLL). For DS-PLL NPs, DS (1.8 mg mL<sup>-1</sup>) and PLL (1 mg mL<sup>-1</sup>) solutions were prepared by dissolving the biopolymers in acetate buffer (0.1 M and pH = 5.5) under magnetic stirring. The solutions were then filtered by using syringe filters (0.22  $\mu$ m, Fisher Scientific, PA) to remove particles, precipitates, and undissolved powders. The PLL solution was then added drop by drop to DS in excess at different polycation : polyanion volume ratios (1 : 5, 1 : 6, 1 : 7 and 1 : 10) under vigorous stirring.

A similar procedure was used for GT-PLL with some modifications. PLL (1 mg mL<sup>-1</sup>) was mixed with GT (1.8 mg mL<sup>-1</sup>) at different polycation : polyanion volume ratios (1 : 5, 1 : 6, 1 : 7 and

1 : 10). The mixtures were left for 24 h to settle and to separate the aggregated part. The supernatant solutions were decanted and centrifuged at 12 000 rpm for 15 min, and finally, the precipitates were freeze-dried (vacuum: 9 Pa, -50 °C; LaBCONCO, USA). The production yield was determined based on the mass of the dried PCNs relative to the dry mass of the starting polymers.

### Material characterization

Size and morphology of the PCN NPs were examined by scanning electron microscopy (SEM, TESCAN, MIRA3, Czech Republic) and transmission electron microscopy (TEM, Zeiss – EM10C). The dried NPs were dispersed in DI water to attain dilute suspensions. For SEM imaging, the suspensions were placed onto aluminum foil and left to dry at room temperature and gold-coated using an Edwards Sputter Coater (DST1-2, Nanostructured Coatings Co., Iran). SEM images were taken at 2 kV. The mean diameter of the NPs was calculated by measuring the diameter of at least 50 random NPs for each sample from their SEM images using Image J software (National Institute of Health, Bethesda, MD).

For TEM imaging, a drop of the diluted suspension was placed on a copper-coated grid (Formvar/carbon 200 mesh, copper), and TEM analysis was performed at 80 kV. The hydrodynamic size distribution of the NPs was determined using dynamic light scattering (Zetasizer Ver. 6.00, MALVERN, UK) in DI water and cell culture media ( $\alpha$ -MEM). The surface charge of the PCNs in DI water at 25 °C was measured using a ZetaPALS instrument (Zetasizer Ver. 6.00, MALVERN, UK) in both DI water and cell culture media ( $\alpha$ -MEM). Fourier transform infrared (FTIR) spectra of the NPs were recorded using a PerkinElmer instrument (RX, USA) between 450 and 4000 cm<sup>-1</sup> with a resolution of 1 cm<sup>-1</sup>.

### Cytocompatibility

HS-5 cells from human bone marrow/stroma (obtained from ATCC, Manassas, USA) were cultured at 37 °C in a 5% CO<sub>2</sub> and humidified atmosphere in Minimum Essential Medium  $\alpha$  ( $\alpha$ -MEM, Gibco, Thermo Fisher Scientific). The medium was supplemented with FBS (10%v/v) and penicillin/streptomycin (1%v/v). At 70% confluency, the cells were used for the evaluation of cell viability and metabolic activity. The biocompatibility of different concentrations of PCNs (200, 400 and 800  $\mu$ g mL<sup>-1</sup>) towards HS-5 cells was evaluated through cell viability and metabolic activity assessments.

To evaluate the cell viability after contact with PCNs, a commercial live/dead assay kit was used.<sup>46,47</sup> To do this, the cells were first seeded in a 24-well plate at a density of 20 000 cells per cm<sup>2</sup>, and then 1 mL of  $\alpha$ -MEM containing 10% FBS was added to each well. The cells were allowed to attach for 4 h. PCNs, DS-PLL, and GT-PLL were then diluted with  $\alpha$ -MEM to 3 different concentrations (200, 400, and 800  $\mu$ g mL<sup>-1</sup>). After cellular attachment, the resulting solutions were added to the cells. The untreated cell-seeded wells were used as the control. The cells were then incubated at 37 °C in 5% CO<sub>2</sub> for 24 h. The media were aspirated, followed by washing three times with DPBS before live/dead staining.

To perform the live/dead assay, the cells were stained with ethidium homodimer-1 (EthD-1,  $2 \mu\text{l ml}^{-1}$  in DPBS) for the dead cells and Calcein AM ( $0.5 \mu\text{l ml}^{-1}$  in DPBS) for the live cells.  $400 \mu\text{L}$  of dye solution was added to each well, and the plates were incubated in the culture incubator for 15 min at  $37^\circ\text{C}$ . For each well, three images were taken by an inverted fluorescence microscope (Zeiss Axio Observer Z1). Live and dead cells were counted using the ImageJ software, and the viability was reported by calculating the number of live cells divided by the total cell number containing live and dead cells.

The measurement of metabolic activity of the cells was performed on days 1, 3, and 5 using a PrestoBlue® assay according to the manufacturer's protocol. Briefly, the cells treated with PCNs were incubated with a solution containing 10% PrestoBlue® reagent and 90% cell culture medium for 45 min at  $37^\circ\text{C}$ . The final fluorescence was recorded at 535–560 nm excitation and 590–615 nm emission. Relative fluorescence values were calculated and reported for each time point.

### Formation of VEGF loaded PCNs

VEGF in DPBS was added to PCN solutions ( $1 \text{ mg mL}^{-1}$ ) to make  $100 \text{ ng mL}^{-1}$  final concentration of the growth factor under stirring for 30 min. The growth factor loaded PCNs were then centrifuged (9000 *ref* for 10 min). The supernatants were diluted to obtain VEGF concentration in the range of the ELISA. To evaluate the VEGF loading efficiency with the PCNs, an ELISA VEGF kit (R&D System, PeproTech, USA) was used. The growth factor bound to PCNs was measured by subtracting the VEGF concentration in the supernatants from the initial loaded VEGF in the solution.

### Culture of HUVECs

HUVECs (CC-2519, Lonza Group, Basel, Switzerland) were cultured at  $37^\circ\text{C}$ , 5%  $\text{CO}_2$ , and humidified atmosphere in EGM-2. The basal medium (not supplemented with VEGF, EGF, bFGF, and IGF) was used to evaluate cell metabolic and mitogenic behavior.

### Pre-conditioning VEGF and VEGF-loaded PCNs

To investigate the capability of the PCNs to immobilize VEGF, VEGF-loaded PCNs and unbound (free) VEGF were first pre-conditioned through incubation in the cell culture media containing 10% FBS at different time points (7, 14, or 21 days and  $37^\circ\text{C}$ ) to destabilize VEGF. Finally, the activity of VEGF was evaluated through investigating the mitosis and metabolic ability of HUVECs in the low serum media to prevent the interaction between the different compositions in the cell culture media with the growth factors that should be tested. The same procedure (described in VEGF loaded PCNs) was used to load VEGF to each PCN type (DS-PLL and GT-PLL) without centrifugation.

### Cell response to unbound VEGF and VEGF-loaded PCNs

To evaluate the ability of PCNs to stabilize the growth factor, HUVECs were cultured in the presence of free and bound VEGF in the low-serum cell culture media. HUVECs' mitogenic

properties were assayed after 48 h of culture using the DAPI staining, imaging and counting the nuclei. Finally, the metabolic activity of treated cells was assessed by the MTT assay after 48 h of culture.

**Mitogenic activity assay.** The HUVEC proliferation assay was performed to indicate the activity of pre-conditioned VEGF after 7 and 14 days in the cell culture media at  $37^\circ\text{C}$ . The cell density was 3000 cells per  $\text{cm}^2$ . Pre-conditioned VEGF-loaded PCNs and free VEGF were both tested. Firstly, the cells were incubated for 2 h to attach to the surface of the plate by adding 0.5 mL of the untreated media containing 10% FBS in a 48-well plate. The seeding media were then aspirated and replaced with 0.5 mL of the low-serum media containing the pre-conditioned VEGF-loaded PCNs and free VEGF. PCN treatments were diluted using the low serum media to  $100 \mu\text{g mL}^{-1}$  (PCN) containing  $10 \text{ ng mL}^{-1}$  VEGF final concentration. Free VEGF treatment was also diluted to  $10 \text{ ng mL}^{-1}$ . The cell nuclei were stained using 4',6-diamidino-2-phenylindole (DAPI). Briefly, the cells were fixed in 4% (v/v) paraformaldehyde (Sigma) for 20 min and then permeabilized with 0.1% (w/v) Triton X-100 solution in DPBS for 45 min. Next, 1% (w/v) bovine serum albumin (BSA) solution in DPBS was used to block the samples for 20 min. The samples were stained with  $1 \mu\text{L mL}^{-1}$  DAPI in DPBS for 5 min and washed three times with DPBS. The stained samples were kept at  $4^\circ\text{C}$  in the dark until taking the images. Three nonoverlapping images were taken from each sample. The ImageJ software (National Institutes of Health, USA) was used to process the images. The cell number per area was calculated by the counting of the cell nuclei using the particle analyzer algorithm in the ImageJ software. Finally, the VEGF activity was recorded as the mean cell number per area of each sample and normalized through the average cells per area in the untreated samples as a control (without VEGF).

**Metabolic activity measurement.** To investigate the effect of VEGF on the cells, the metabolic activity of the cells were evaluated by MTT assays at days 7, 14, and 21 after preconditioning periods. All treatments were conducted in triplicate with the cell seeding density of  $10^4$  cells per  $\text{cm}^2$ . The cells were incubated for 2 h to attach to the surface of the well plates with 0.5 mL of the non-treated media supplemented with 10% FBS. The media were taken and replaced with 0.5 mL of the low-serum media containing the treatment (preconditioned VEGF bound to each type of PCNs and free VEGF). All treatments were added to the media to obtain the same final concentrations in the mitosis assay as explained before. The MTT assay was performed according to the manufacturer's instructions after 48 h of culture. Finally, the VEGF activity was reported as the average of all readings for each sample and then normalized based on the negative control (no VEGF).

## Conclusions

The biomimetic proteoglycan PCNs were developed using a polymer–polymer pair interaction based on cationic (PLL) and

anionic (DS and GT) polymers with no use of crosslinker, surfactant and organic solvents or further chemical functionalization to bind the growth factor. The negatively charged PCNs can easily bind to the positively charged drug and growth factors, which makes them suitable candidates for the delivery of therapeutics. It was shown that at concentrations of 200  $\mu\text{g mL}^{-1}$  and above, the NPs could prevent attachment of the cells to well plates, and at higher concentrations, they may show cytotoxic effects toward HS-5 cells. The result also determined the time- and dose-dependent HS-5 cells' metabolic activity.

The results confirmed that the mitogenic activity of VEGF was maintained after binding well to DS-PLL PCNs. Free VEGF in solution did not show significant mitogenic properties during all incubation periods. Additionally, during the equal pre-conditioning time periods, delivery of VEGF using both types of PCNs showed a higher metabolic activity compared to free VEGF. This could enhance the prospects for the delivery of therapeutics using nanoparticle immobilized growth factors or cytokines for tissue regeneration applications.

## Conflicts of interest

There are no conflicts to declare.

## Acknowledgements

AS wishes to acknowledge the funding support from Sharif University of Technology (Grant No. QA970816) and Iran National Science Foundation (INSF No. 95-S-48740). NA acknowledges the support from National Institutes of Health (NIH) (R01EB023052; R01HL140618).

## References

- M. Uehara, X. Li, A. Sheikhi, N. Zandi, B. Walker, B. Saleh, N. Banouni, L. Jiang, F. Ordikhani and L. Dai, *Sci. Rep.*, 2019, **9**, 6535.
- V. Bourganis, T. Karamanidou, O. Kammona and C. Kiparissides, *Eur. J. Pharm. Biopharm.*, 2017, **111**, 44–60.
- R. K. Das, N. Kasoju and U. Bora, *Nanomedicine*, 2010, **6**, 153–160.
- Y. A. Shchipunov and I. V. Postnova, *Compos. Interfaces*, 2009, **16**, 251–279.
- Q. Hu, T. Wang, M. Zhou, J. Xue and Y. Luo, *Int. J. Biol. Macromol.*, 2016, **92**, 812–819.
- R. Poojari, S. Kini, R. Srivastava and D. Panda, *Colloids Surf., B*, 2016, **143**, 131–138.
- E. Mostafavi, P. Soltantabar and T. J. Webster, Nanotechnology and picotechnology: A new arena for translational medicine, in *Biomaterials in Translational Medicine*, Academic Press, 2019, pp. 191–212.
- F.-G. Wu, Y.-W. Jiang, Z. Chen and Z.-W. Yu, *Langmuir*, 2016, **32**, 3655–3664.
- J.-F. Gohy, S. K. Varshney and R. Jérôme, *Macromolecules*, 2001, **34**, 2745–2747.
- M. M. Stevens and J. H. George, *Science*, 2005, **310**, 1135–1138.
- Y. Parajó, I. d'Angelo, A. Welle, M. Garcia-Fuentes and M. J. Alonso, *Drug Delivery*, 2010, **17**, 596–604.
- S. Kaihara, Y. Suzuki and K. Fujimoto, *Colloids Surf., B*, 2011, **85**, 343–348.
- A. Anitha, V. Deepagan, V. D. Rani, D. Menon, S. Nair and R. Jayakumar, *Carbohydr. Polym.*, 2011, **84**, 1158–1164.
- M. A. Shahbazi, M. Hamidi and S. Mohammadi-Samani, *J. Pharm. Pharmacol.*, 2013, **65**, 1118–1133.
- C. Tan, J. Xie, X. Zhang, J. Cai and S. Xia, *Food Hydrocolloids*, 2016, **57**, 236–245.
- U. Lindahl and L. Kjellén, *J. Intern. Med.*, 2013, **273**, 555–571.
- D. M. Copolovici, K. Langel, E. Eriste and U. Langel, *ACS Nano*, 2014, **8**, 1972–1994.
- G. Frescaline, T. Boudierlique, M. B. Huynh, D. Papy-Garcia, J. Courty and P. Albanese, *Stem Cell Res.*, 2012, **8**, 180–192.
- R. Duschinsky and E. Plevin, *J. Am. Chem. Soc.*, 1957, **79**, 4459–4463.
- D. Berry, C.-P. Kwan, Z. Shriver, G. Venkataraman and R. Sasisekharan, *FASEB J.*, 2001, **15**, 1422–1424.
- S. Boddohi and M. J. Kipper, *Adv. Mater.*, 2010, **22**, 2998–3016.
- A. Papagiannopoulos, T. Waigh, T. Hardingham and M. Heinrich, *Biomacromolecules*, 2006, **7**, 2162–2172.
- C. B. Knudson and W. Knudson, *Semin. Cell Dev. Biol.*, 2001, **12**, 69–78.
- J. J. Zoeller, J. M. Whitelock and R. V. Iozzo, *Matrix Biol.*, 2009, **28**, 284–291.
- A. Nasirpour, M. Amir, Z. Hajhashemi and M. Fazilati, *Int. Food Res. J.*, 2013, **20**, 1249–1254.
- M. A. Mohammadifar, S. M. Musavi, A. Kiumarsi and P. A. Williams, *Int. J. Biol. Macromol.*, 2006, **38**, 31–39.
- J. Kuchlyan, D. Banik, A. Roy, N. Kundu and N. Sarkar, *J. Phys. Chem. B*, 2015, **119**, 8285–8292.
- B. Sarmiento, A. Ribeiro, F. Veiga and D. Ferreira, *Colloids Surf., B*, 2006, **53**, 193–202.
- A. Mohandas, B. Anisha, K. Chennazhi and R. Jayakumar, *Colloids Surf., B*, 2015, **127**, 105–113.
- Y. Wen, L. Grøndahl, M. R. Gallego, L. Jorgensen, E. H. Møller and H. M. Nielsen, *Biomacromolecules*, 2012, **13**, 905–917.
- Q. Tan, H. Tang, J. Hu, Y. Hu, X. Zhou, Y. Tao and Z. Wu, *Int. J. Nanomed.*, 2011, **6**, 929.
- S. Rodrigues, M. Dionísio, C. R. López and A. Grenha, *J. Funct. Biomater.*, 2012, **3**, 615–641.
- M. Huang, S. N. Vitharana, L. J. Peek, T. Coop and C. Berkland, *Biomacromolecules*, 2007, **8**, 1607–1614.
- N. Perrimon and M. Bernfield, *Nature*, 2000, **404**, 725.
- S. D. Kingma, T. Wagemans, L. IJlst, A. L. Bronckers, T. H. van Kuppevelt, V. Everts, F. A. Wijburg and N. van Vlies, *Bone*, 2016, **88**, 92–100.
- J. J. Green and J. H. Elisseeff, *Nature*, 2016, **540**, 386.

- 37 S. Safi, M. Morshed, S. Hosseini Ravandi and M. Ghiaci, *J. Appl. Polym. Sci.*, 2007, **104**, 3245–3255.
- 38 M. Rozenberg and G. Shoham, *Biophys. Chem.*, 2007, **125**, 166–171.
- 39 A. F. Martins, J. F. Piai, I. T. Schuquel, A. F. Rubira and E. C. Muniz, *Colloid Polym. Sci.*, 2011, **289**, 1133–1144.
- 40 D.-W. Tang, S.-H. Yu, Y.-C. Ho, F.-L. Mi, P.-L. Kuo and H.-W. Sung, *Biomaterials*, 2010, **31**, 9320–9332.
- 41 Y.-L. Chen, H.-P. Lee, H.-Y. Chan, L.-Y. Sung, H.-C. Chen and Y.-C. Hu, *Biomaterials*, 2007, **28**, 2294–2305.
- 42 M. G. Sankalia, R. C. Mashru, J. M. Sankalia and V. B. Sutariya, *Eur. J. Pharm. Biopharm.*, 2007, **65**, 215–232.
- 43 E. Kokufuta, K. Ogawa, R. Doi, R. Kikuchi and R. S. Farinato, *J. Phys. Chem. B*, 2007, **111**, 8634–8640.
- 44 M. Lyon, J. A. Deakin, K. Mizuno, T. Nakamura and J. T. Gallagher, *J. Biol. Chem.*, 1994, **269**, 11216–11223.
- 45 E. Wijelath, M. Namekata, J. Murray, M. Furuyashiki, S. Zhang, D. Coan, M. Wakao, R. B. Harris, Y. Suda and L. Wang, *J. Cell. Biochem.*, 2010, **111**, 461–468.
- 46 E. Shirzaei Sani, R. Portillo-Lara, A. Spencer, W. Yu, B. M. Geilich, I. Noshadi, T. J. Webster and N. Annabi, *ACS Biomater. Sci. Eng.*, 2018, **4**, 2528–2540.
- 47 E. S. Sani, A. Kheirkhah, D. Rana, Z. Sun, W. Foulsham, A. Sheikhi, A. Khademhosseini, R. Dana and N. Annabi, *Sci. Adv.*, 2019, **5**, eaav1281.